X-ray diffraction imaging of dislocation generation related to microcracks in Si wafers

J. Wittge and A. Danilewsky
Kristallographie, Geowiss. Institut, University Freiburg, Freiburg, Germany

D. Allen and P. McNally
Research Institute for Networks and Communications Engineering, Dublin City University, Dublin, Ireland

Z. J. Li and T. Baumbach
Research Centre Karlsruhe, Institut für Synchrotronstrahlung, Karlsruhe, Germany

E. Gorostegui-Colinas, J. Garagorri, and M. R. Elizalde
Centro de Estudios e Investigaciones Tecnicas de Gipuzkoa, San Sebastian, Spain

D. Jacques
Jordan Valley Semiconductor (UK), Durham DH1 1TW, United Kingdom

M. C. Fossati, D. K. Bowen, and B. K. Tanner[a)]
Department of Physics, Durham University, South Road, Durham DH1 3LE, United Kingdom

(Received 22 February 2010; accepted 24 February 2010)

The nucleation of dislocations at indents in silicon following rapid thermal annealing (RTA) has been examined by X-ray diffraction imaging (topography). For indentation loads below 200 mN, no slip bands were generated from the indent sites following RTA at 1000 °C under spike conditions. Upon plateau annealing at 1000 °C, slip dislocations were propagated from some indents but not all. Slip was also observed from edge defects not associated with indentation. For 500-mN indentation load, large scale dislocation sources were generated from the indent sites propagating on two of the four {111} slip planes. These dislocations multiplied into macroscopic-scale slip bands. A significant change in morphology was observed in the 60° dislocation segments after the screw segment reached the rear surface of the wafer. Dislocations changed line direction and in some cases appeared to leave the Peierls trough during glide. © *2010 International Centre for Diffraction Data.* [DOI: 10.1154/1.3392369]

Key words: X-ray diffraction imaging, topography, dislocation source

I. INTRODUCTION

Wafer handling in semiconductor manufacturing introduces microcracks at the wafer edge. Most are harmless, but if the gripper is out of adjustment or damaged, during (rapid) thermal processing some of these microcracks generate slip bands which can result in device yield loss by locally increasing the diffusion coefficients for dopants. More importantly cracks may grow catastrophically shattering the wafer and disrupting manufacture. Alternatively, as a slip band that ends inside a bounded solid has a stress field similar to that of a wedge or shear disclination this will be liable to expand catastrophically if the gradient-induced stresses built up by rapid thermal annealing (RTA) cannot be relieved by slip. The slip band itself may act as a crack nucleus or it may activate other local nuclei. Typically, up to two days production is lost in cleaning the relevant production tool, and, since the shattering normally occurs in a tool remote from the one containing the faulty gripper, diagnosing the root cause of the problem can be a time consuming and expensive process. The typical loss of wafers through breakage is of the order of €2 m per annum for a single fabrication line. (International SEMATECH Manufacturing Initiative, Industry Economic Model v8.1ss 2004; annualized value based on a fab operating at 20 000 300-mm wafers per month producing custom products in 180 to 90 nm technology. Note that the value of product lost increases approximately as the inverse square of the node dimension.) There are relatively few papers in the literature treating the subject of wafer breakage. Recent work has been on edge-defined film-fed growth (EFG) wafers for solar cell applications (Brun and Melkote, 2006; Brun and Melkote, 2009). These authors modelled the total stress state in the wafer and related this to the crack size and position which resulted in fracture. They used indentation to verify the conclusion that the wafer breakage stress during handling is proportional to the inverse square root of the crack length, consistent with linear elastic fracture mechanics theory. Theoretical modelling of the strength of brittle material with the surface, bulk, and edge microcracks has also been compared with data on silicon for photovoltaic devices (Rupnowski and Spoori, 2009). Empirical work on silicon substrates for integrated circuit manufacture has focused on the design of the edge profile to minimise the effects of edge microcracks (Chen *et al.*, 2007).

X-ray diffraction imaging (XRDI), often referred to as X-ray topography, is capable of imaging microcracks and slip bands with very high strain sensitivity (Bowen and Tanner 1998, 2006). The aim of the SIDAM project, supported by the European Commission, is to discover how to derive quantitative predictive information from the X-ray images

[a)]Author to whom correspondence should be addressed. Electronic mail: b.k.tanner@durham.ac.uk

about which defects are probably going to be critical and thus to enable a new metrology of wafer inspection.

II. METHODS

Vickers indentation has been shown as a valuable tool to introduce controlled flaws in Si that emulate well those that have arisen during the processing of Si wafers (Cook, 2006). We have started at very small indentation loads and used a Berkovich diamond tip on an Agilent Nanoindenter II (located at CEIT, San Sebastian) to introduce controlled amounts of local damage into 200-mm device-grade (100) silicon wafers. Groups of three indents, separated by 1 mm, were placed close to the bevel edge at 30° intervals around the wafer. Indent loads discussed in this paper were 200 or 500 mN.

RTA was performed at CEIT on a JetFirst 200 purchased from Qualiflow Therm-Jipelec. Two annealing schemes were used shown in Figure 1. In both cases, the heating time to 1000 °C was 10 s and cooling achieved under forced gas convection. In the spike annealing procedure [Figure 1(a)], cooling began immediately on reaching 1000 °C, while the plateau annealing [Figure 1(b)] involved holding the temperature at 1000 °C for 60 s prior to cooling.

XRDI measurements were made at Jordan Valley Semiconductors (U.K.) using the BedeScan™ tool shown in Figure 2 (Bowen *et al.*, 2003) and with the white beam from the TOPO-TOMO beamline (Figure 3) (Danilewsky *et al.*, 2003) at the ANKA synchrotron radiation source at the Institute for Synchrotron Radiation Studies, Forschungszentrum Karlsruhe, Germany. In both cases the transmission mode was used. The BedeScan™ tool was operated with a detector resolution of 10 μm, and at ANKA, images were recorded on Slavich VRP-M films with a grain size of about 0.04 μm.

III. RESULTS AND DISCUSSION

The diffraction images of the as-received wafers taken with the BedeScan™ tool (Figure 4) showed only very few small defects close to the wafer rim. An example is the black feature shown in the expanded scale view of the region close to the orientation notch. Prominent on the image is the wafer number laser-scribed onto the surface demonstrating that significant strain remains present around the numbers. High resolution images taken at ANKA reveal that the numbers are made up of discrete dots, each showing contrast not dissimilar to that from indents.

Indentation produces images which scale in size with the indenter load and which show almost no anisotropy with respect to the wafer orientation (Allen *et al.*, 2010). There is good qualitative agreement with the features in the von Mises stress profiles around the indentations simulated using finite element methods.

Figure 5(a) shows the images of 200-mN load indents in a wafer which has had no heat treatment. The indents are separated by 1 mm and placed diametrically opposite the notch as close as possible to the start of the bevel on the wafer edge, the latter being revealed by the thickness fringes that run parallel to the thickness contours. The characteristic lobed images are elongated, but this is an X-ray optical effect rather than an evidence of asymmetry in the strain field. Note that even in the unprocessed wafer, there are quite a number of images of spherical strain centres, characterised by their black-white half-moon contrast, present within this relatively small field of view. Spike annealing [Figure 5(b)] results in no dislocation nucleation at 200-mN indents identically located opposite the notch just before the start of the bevel. There are now more extraneous defects but no indications of slip. Indeed, whole wafer scans show equivalent BedeScan™ images to that of Figure 4.

Plateau annealing results in no nucleation of slip from equivalent 200-mN indents placed again at 180° azimuth to the notch position. However, there is present within the field of view a single dislocation. The sharp image at its right hand end indicates that this marks the intersection of the dislocation line with the exit surface in the transmission diffraction geometry. Its length, projected into the diffraction vector direction shows that it lies on an inclined {111} plane. The image is diffuse towards the intersection with the X-ray entrance surface due to the relatively long wavelength that the crystal has selected in this instance. This, together with the beaded contrast close to the intersection with the exit surface, is characteristic of dislocation images taken under conditions where the product of the absorption coefficient (μ) and thickness (t) is somewhat greater than unity (i.e., $\mu t > 1$).

An inspection of the complete plateau annealed wafer (Figure 6) shows that the region opposite the notch (at the top of the image in the case) is indeed free from slip bands. However, this is not the case for the rest of the perimeter of the wafer. Substantial slip has occurred, it being predominant in the regions corresponding to the [001] and [010] directions in the wafer. Relatively little slip is seen in the [011] and $[01\bar{1}]$ directions. There is no correlation between the origin of slip and the 200-mN indentations and it is impossible to determine which edge defects, previously revealed in our incoming wafer screening process, resulted in slip nucleation.

Increasing the load to 500 mN had a huge effect on the indents after plateau annealing. While substantial slip was still observed from unidentified defects at the wafer edge, some indents had acted as the generation point for spectacular sources reminiscent of Frank–Read (Figure 7). We believe this to be the first time that such clear dislocation sources of this size have been identified with a known and controlled nucleation site. They are comparable in size and clarity to the beautiful, but elusive, double ended Frank–Read sources produced in carefully controlled torsion conditions by Dash almost half a century ago (Dash, 1956).

The sources operate on the inclined $(1\bar{1}1)$ and $(11\bar{1})$ slip planes containing the [011] direction in the surface of the wafer. Of the three indents in the field of view in Figure 7, the indent on the right has an obvious source associated with it while the left hand indent has generated a dense slip band presumably by the operation of sources such as that on the right of the image. The central indent appears to have no source related to it, but a careful examination of another reflection does reveal that there is a short dislocation loop just emerging from the indent site. The annealing conditions and the load appear to be just at the threshold for extensive source operation and slip band densification. We noted elsewhere (Allen *et al.*, 2010) that the contrast around nominally

https://doi.org/10.1154/1.3392369 Published online by Cambridge University Press

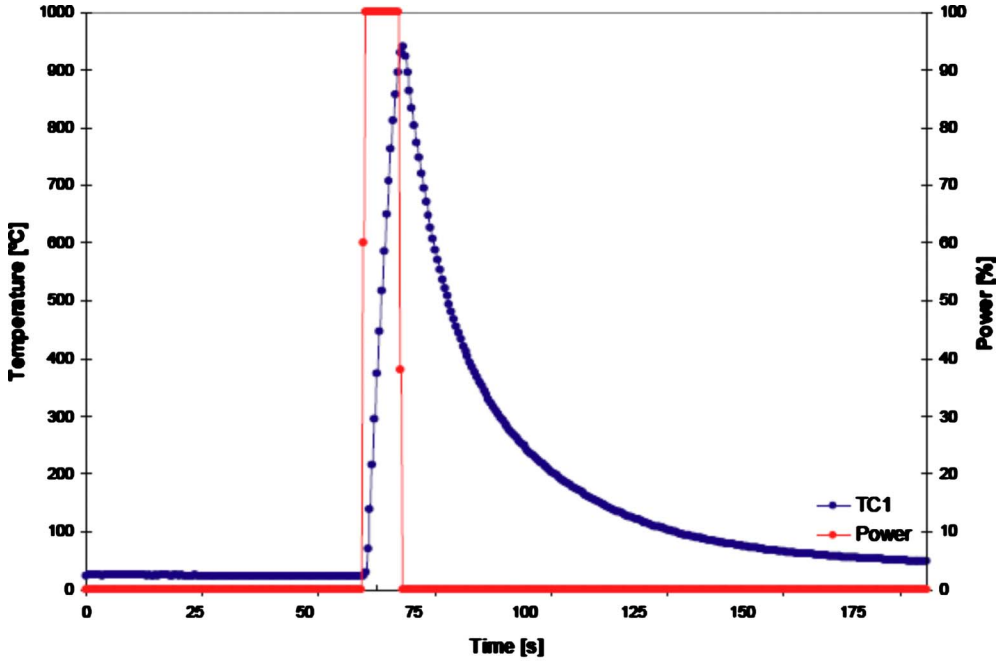

- **Heating up to 941 °C in 8 seconds.**
- **Cooling: forced convection under 2900 sccm He gas flow.**

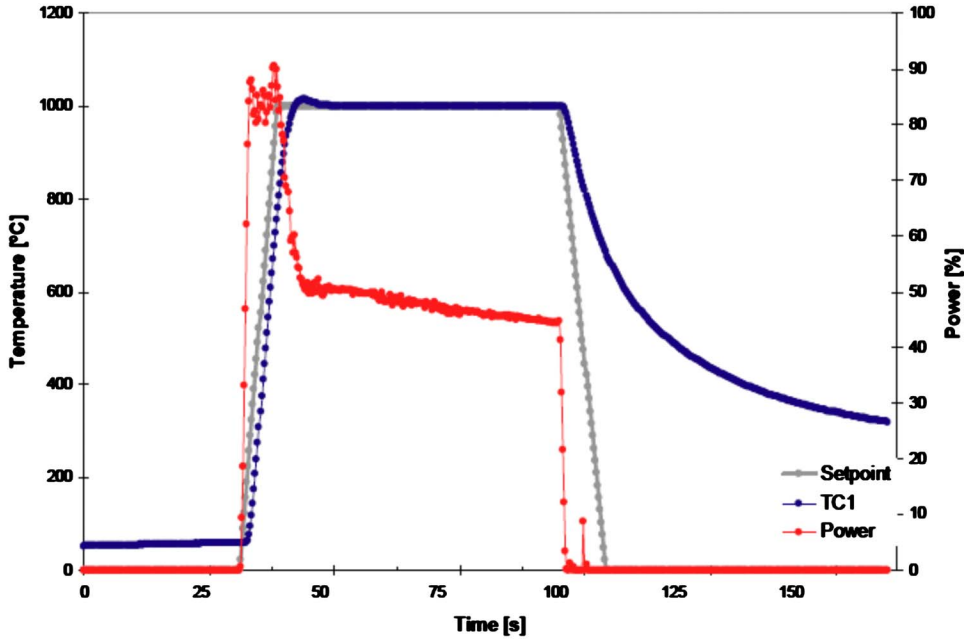

- **Heating up to 1000 °C in 10 seconds.**
- **Plateau for 60 seconds at 1000 °C.**
- **Cooling: forced convection under 1500 sccm N_2 gas flow.**

Figure 1. (Color online) (a) Spike annealing sequence. (b) Plateau annealing sequence.

identical indents varied considerably, probably associated with the stochastic nature of the breakout of material at the indenter tip and it is therefore unsurprising that the three sources behave somewhat differently.

The indent to the right shows most clearly the mechanism of source operation. This appears to be a simple punching out of dislocation loops from the surface on the inclined slip planes. There appears to be no dislocation loop operating as would be the case of a single-ended Frank–Read source. The sources of the left hand slip band associated with this indent have poor quality contrast and are difficult to resolve in stark contrast to the right hand slip band. We note that the Burgers vector of loops punched out on this slip plane will have the opposite sense Burgers vector to those of the well-resolved source. Due to the significant displacement of the film from the sample in synchrotron radiation X-ray topog-

https://doi.org/10.1154/1.3392369 Published online by Cambridge University Press

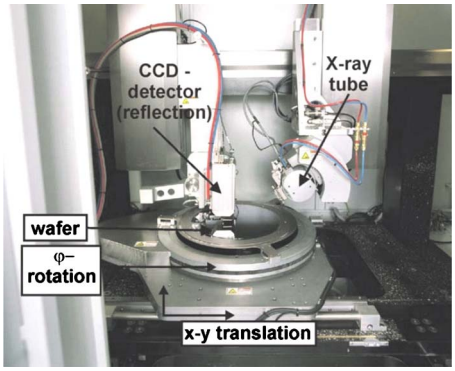

Figure 2. (Color online) BedeScan™ X-ray diffraction imaging system (in reflection geometry configuration).

raphy, the orientation contrast associated with the dislocation may result in the two sides of the image either converging or diverging with distance from the sample (Midgley *et al.*, 1977). One sense of the Burgers vector (diverging image) remains sharp while the other (converging image) becomes diffuse and hard to detect above the contrast from the perfect crystal. The characteristic of the diverging image is its bimodal profile visible in the enlarged inset of Figure 7.

The inclined dislocation segments all intersect the (100) surface in a line in the [011] direction except in the region above the indent. Here the intersections make a characteristic

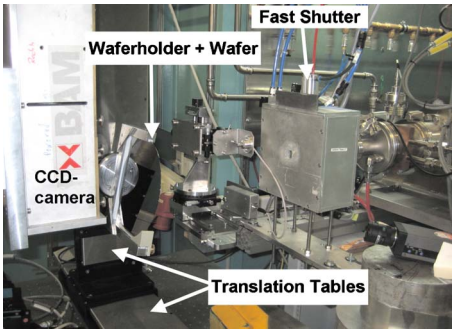

Figure 3. (Color online) X-ray diffraction imaging system on the TOPO-TOMO beamline at ANKA.

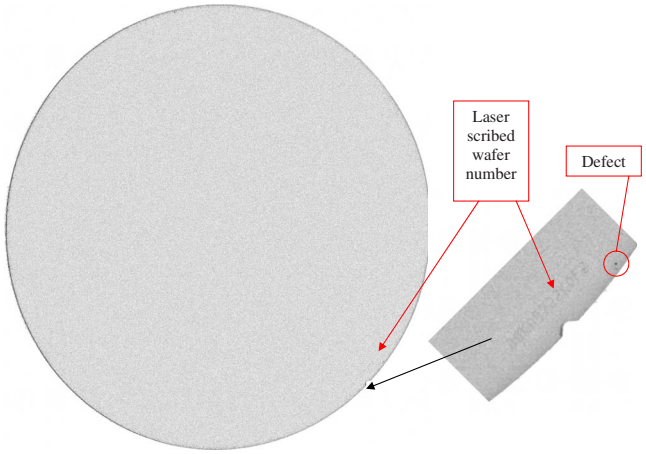

Figure 4. (Color online) BedeScan™ image of an as-received 200-mm diameter wafer. 004 reflection, Mo $K\alpha$ radiation. Diffraction vector horizontal. (100) wafer, notch ⟨011⟩.

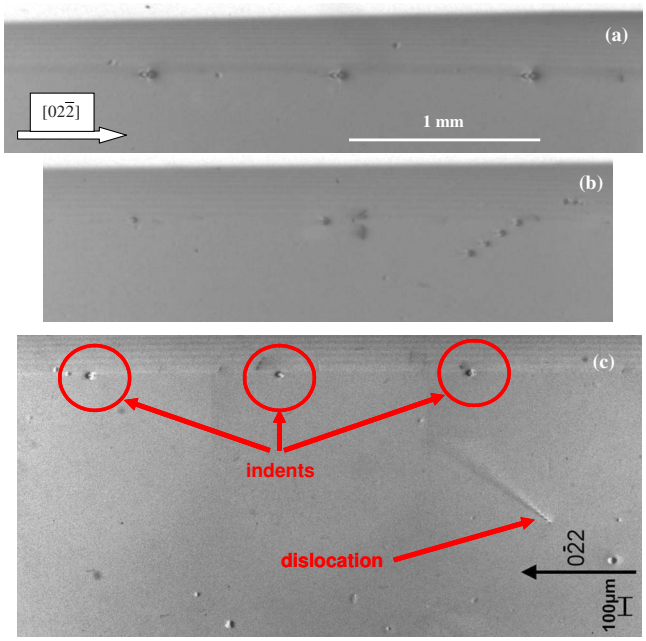

Figure 5. (Color online) White beam synchrotron radiation images of 200-mN load indents (a) unannealed, (b) spike annealed, and (c) plateau annealed. [In (a) and (b) the diffraction vector points towards the right; in (c) it is reversed and points to the left. As a result, the black-white contrast of the defects is reversed.]

"V" shape which is also prominent in the slip bands associated with the left hand indent. This has no fundamental significance and is simply an artefact associated with the bevel at the edge of the wafer. The indents were placed as close as possible to the start of the edge bevel, whose existence can just be made out by the weak thickness fringes associated with it. On the other hand, the change in shape of the inclined segment of the dislocation when the [001] segment of the dislocation disappears is significant. The inclined segment appears to be pinned by the dislocations on the other slip system where it intersects the surface. Initially, when the

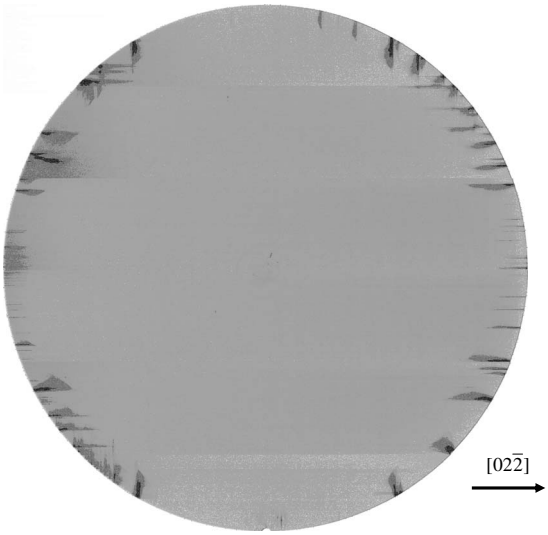

Figure 6. BedeScan™ image of the full 200-mm wafer that had been subjected to plateau annealing. 02$\bar{2}$ reflection, Mo $K\alpha$ radiation. (100) wafer, notch ⟨011⟩.

https://doi.org/10.1154/1.3392369 Published online by Cambridge University Press

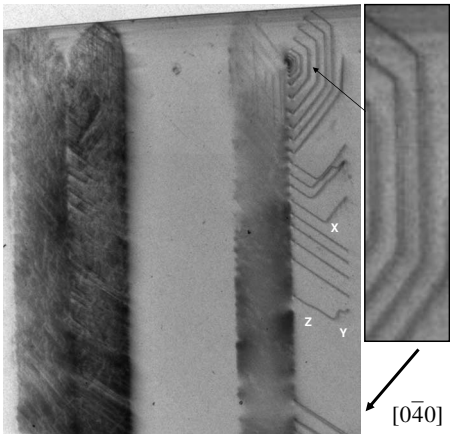

Figure 7. Transmission white beam image of slip bands and dislocation sources associated with 500-mN indents after plateau annealing. 0$\bar{4}$0 reflection.

full half loop is present there is a short segment running in the $[1\bar{1}0]$ and a long one in the $[101]$ direction. When the $[011]$ segment is lost, the $[101]$ segment increases in length due to the higher velocity of the $[1\bar{1}0]$ segment, which is now unpinned. Eventually the $[101]$ segment, which is impeded by the interaction with the dislocations on the left hand slip plane, extends all the way along the dislocation line, which is therefore straight. At *Y* such a straight dislocation seems to have been pinned at the surface, as it has kinked and although remaining on the slip plane, has come out of its Peierls trough to begin the process of bypassing the defect by the creation of a dislocation loop. The dislocation also has left the Peierls trough at *Z* as a result of the creation of this deformation.

IV. CONCLUSION

On thermal annealing at 1000 °C, 500-mN indents create dislocation sources that propagate across the wafer. Below 200-mN load, no such sources are generated putting some limits on the damage levels that result in the formation of slip in silicon wafers during processing. This is in good agreement with results from slow thermal annealing measurements (Danilewsky *et al.*, 2010) where after 60 min also no slip bands, but some straight dislocations were created already at temperatures below 800 °C.

ACKNOWLEDGMENTS

This work was supported by the European Community Research Infrastructure Action under FP7 "Structuring the European Research Area" programme. Financial support was provided through EU-FP7 Project No. 216382 SIDAM.

Allen, D., Wittge, J., Zlotos, A., Gorostegui-Colinas, E., Garagorri, J., Mcnally, P. J., Danilewsky, A. N., and Elizalder, M. R. (**2010**). "Observation of nano-indent induced strain fields and dislocation generation in silicon wafers using micro-Raman spectroscopy and white beam X-ray topography," Nucl. Instrum. Methods Phys. Res. B **268**, 383–387.

Bowen, D. K. and Tanner, B. K. (**1998**). *High-Resolution X-ray Diffraction and Topography* (Taylor and Francis, London).

Bowen, D. K. and Tanner, B. K. (**2006**). *X-ray Metrology in Semiconductor Manufacturing* (CRC/Taylor and Francis, Boca Raton/London).

Bowen, D. K., Wormington, M., and Feichtinger, P. (**2003**). "A novel digital X-ray topography system," J. Phys. D **36**, A17–23.

Brun, X. F. and Melkote, S. N. (**2006**). "Evaluation of handling stresses applied to EFG silicon wafer using a Bernoulli gripper," *Conference Record of 2006 IEEE Fourth World Conference on Photovoltaic Energy Conversion*, pp. 1346–1349.

Brun, X. F. and Melkote, S. N. (**2009**). "Analysis of stresses and breakage of crystalline silicon wafers during handling and transport," Sol. Energy Mater. Sol. Cells **93**, 1238–1247.

Chen, P. Y., Chen, S. L., Tsai, M. H., Jing, M. H., and Lin, T. C. (**2007**). "Investigation of wafer strength in 12 inch bare wafer for preventing wafer breakage," *IEEE International Conference on Electron Devices and Solid-State Circuits*, pp. 545–548.

Cook, R. F. (**2006**). "Strength and sharp contact fracture of silicon," J. Mater. Sci. **41**, 841–872.

Danilewsky, A., Wittge, J., Hess, A., Cröll, A., Allen, D., McNally, P., Vagoviče, P., Cecilia, A., Li, Z., Baumbach, T., Gorostegui-Colinas, E., and Elizalde, M. R. (**2010**). "Dislocation generation related to microcracks in Si-wafers: High temperature *in situ* study with white beam X-ray topography," Nucl. Instrum. Methods Phys. Res. B **268**, 399–402.

Danilewsky, A. N., Simon, R., Fauler, A., Fiederle, M., and Benz, K. W. (**2003**). "White beam X-ray topography at the synchrotron light source ANKA, Research Centre Karlsruhe," Nucl. Instrum. Methods Phys. Res. B **199**, 71–74.

Dash, W. C. (**1956**). "Copper precipitation on dislocations in silicon," J. Appl. Phys. **27**, 1193–1195.

Tanner, B. K., Midgley, D., and Safa, M., (**1977**). "Dislocation contrast in X-ray synchrotron topographs," J. Appl. Crystallogr. **10**, 281–286.

Rupnowski, P. and Spoori, B. (**2009**). "Strength of silicon wafers: Fracture mechanics approach," Int. J. Fract. **155**, 67–74.